Stick-Slip Dynamics of Moiré Superstructures in Polycrystalline 2D Material Interfaces

Xiang Gao, Michael Urbakh,* and Oded Hod

Department of Physical Chemistry, School of Chemistry, The Raymond and Beverly Sackler Faculty of Exact Sciences and The Sackler Center for Computational Molecular and Materials Science, Tel Aviv University, Tel Aviv 6997801, Israel

(Received 23 March 2022; accepted 6 December 2022; published 29 December 2022)

A new frictional mechanism, based on collective stick-slip motion of moiré superstructures across polycrystalline two-dimensional material interfaces, is predicted. The dissipative stick-slip behavior originates from an energetic bistability between low- and high-commensurability configurations of large-scale moiré superstructures. When the grain boundary separates between grains of small and large interfacial twist angle, the corresponding moiré periods are significantly different, resulting in forbidden grain boundary crossing of the moiré superstructures during shear induced motion. For small twist angle grains, where the moiré periods are much larger than the lattice constant, this results in multiple reflections of collective surface waves between the surrounding grain boundaries. In combination with the individual grain boundary dislocation snap-through buckling mechanism dominating at the low normal load regime, the friction exhibits nonmonotonic behavior with the normal load. While the discovered phenomenon is demonstrated for *h*-BN/graphene polycrystalline junctions, it is expected to be of general nature and occur in many other large-scale layered material interfaces.

DOI: 10.1103/PhysRevLett.129.276101

Van der Waals (vdW) heterojunctions formed by two-dimensional (2D) layered materials exhibit unique electronic [1–4], optical [5,6], mechanical [7–10], and tribological properties [11–15]. Featured by weak interlayer dispersive interactions and an intrinsic lattice mismatch (e.g., ∼1.8% between hexagonal boron nitride (*h*-BN) and graphene (Gr)), high friction commensurate states, such as those found in homogeneous layered interfaces, may be inherently eliminated in their heterogeneous counterparts, thus enabling robust structural superlubricity [12]. The concept has been recently demonstrated by experiments of monocrystalline heterojunctions such as *h*-BN/Gr, molybdenum disulfide (MoS_2)/Gr, and MoS_2/*h*-BN up to the microscale [13,15]. However, aiming to achieve structural superlubricity at increasing length scales, unavoidable grain boundaries (GBs) should be considered.

For a polycrystalline sample, e.g., polycrystalline graphene (PolyGr), the randomness in grain orientation and shape enhances interfacial incommensurability thus promoting the robustness of superlubricity [16]. Nonetheless, the seamline GBs may significantly enhance frictional dissipation [17–19] via dynamic buckling of GB protrusions [20] and may contribute to the breakdown of structural superlubricity for nanoparticles sliding on compliant substrates [21,22]. When polycrystalline layers are further incorporated within a heterogeneous layered interface (e.g., *h*-BN/PolyGr) or an incommensurate (e.g., twisted) homogeneous interface, moiré superstructures naturally appear in the reconstructed lattice. These are characterized by well-defined periodic patterns of flat commensurate domains, separated by elevated ridges, where tensile and compressive in-plane strain accumulate [23,24]. Across the GBs, moiré superstructures of different periods and orientations meet. The application of interlayer lateral sliding results in a collective motion of the moiré superstructures within each grain. Because of symmetry restrictions, however, these moiré superstructures are forbidden to cross the GBs, resulting in their reflection, annihilation, or nucleation at the intergrain seamlines. This, in turn, involves intricate strain accumulation and release processes that generate additional interfacial energy dissipation, leading to unique unexplored frictional behaviors. In this Letter, we reveal the dynamical characteristics of such superstructure scattering at surface GBs and their consequential effects on the frictional properties of heterogeneous polycrystalline layered material interfaces, such as that formed between *h*-BN and PolyGr.

Our model system for the *h*-BN/PolyGr heterojunction shown in Fig. 1(a) is constructed from a six-layer thick stack including, from top to bottom, three layers of pristine *h*-BN, one layer of PolyGr and two layers of pristine graphene (PrisGr). Periodic boundary conditions are applied along both lateral directions. The PolyGr layer is constructed via a Voronoi tessellation method developed by Shekhawat *et al.* [25,26] (see Ref. [20] for further details). As shown in Fig. 1(b), the PolyGr layer contains two grains (marked as grains 1 and 2) separated by two GBs (termed GB 1 and 2). The orientation angles of the two grains, defined by the angle formed between the grain lattice armchair direction and the armchair direction of the pristine Bernal (*AB*) stacked graphene and *AA′* stacked *h*-BN layers (chosen as the *x* axis), are $\theta_1 = 0°$, and $\theta_2 = 8°$ for grains 1

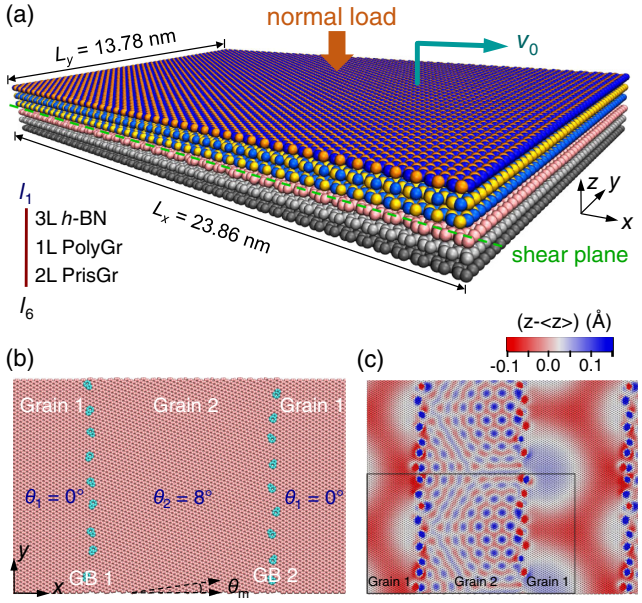

FIG. 1. Model system setup. (a) Perspective view of the h-BN/PolyGr heterojunction. From top to bottom, the system consists of a three-layer-thick h-BN slider (blue and yellow or orange spheres), one layer of PolyGr (pink and cyan spheres), and two-layer-thick PrisGr (gray spheres). The darker colors in the top and bottom layers indicate their rigidity. The shear plane is denoted by the dashed green line. (b) The atomic structure of the PolyGr layer. The left and right sections of grain 1 are connected by periodic boundary conditions. The two dashed-line arrows show the misfit angle θ_m between the grains. The pink and cyan spheres represent the hexagonal and the pentagon-heptagon pair atoms, respectively. (c) Color map of the relaxed topography of the PolyGr layer extracted from panel (a). The black line frames the primary simulation cell, the rest being its periodic replicas shown for clarity of the representation. In the scale bar, z represents the atomic height and $\langle z \rangle$ is the average height of the two grains.

and 2, respectively, giving an inter-GB misfit angle of $\theta_m = 8°$. Note that the choice of a single grain boundary model is well justified as we focus on moiré superstructure dynamics, whose typical dimensions (∼13.9 nm [24]) in aligned or marginally twisted graphene and h-BN interfaces (where its frictional impact is maximal) are considerably smaller than the typical grain boundary length (∼100 nm [27]) found in polycrystalline graphene surfaces.

Intralayer interactions are described with the REBO potential [28] for graphene and the Tersoff potential [29] for h-BN. Interlayer interactions are treated using the large-scale atomic/molecular massively parallel simulator (LAMMPS) implementation of the registry-dependent interlayer potential (ILP) [30–37].

The relaxed topography of the PolyGr surface within the heterojunction exhibits complex out-of-plane distortions [Fig. 1(c)]. To partially relieve the introduced in-plane strain, the pentagon-heptagon pair dislocations at the GBs form upward or downward protrusions (mainly at the pentagon location) with an average corrugation of ∼0.5 Å for the $\theta_m = 8°$ system at zero normal load. Placing the pristine h-BN stack atop the PolyGr surface results in the appearance of moiré superstructures above the two grains. Over grain 1, which is aligned (zero twist angle) with the h-BN lattice, a large moiré period of $\lambda_m \approx 14$ nm is found, where in the blue domains the graphene layer stretches to adapt to the h-BN lattice, whereas in the red grooves it compresses and looses commensurability. On grain 2, a more complex picture appears, as the lattice of the grain is twisted with respect to both the pristine graphitic substrate and the overlying h-BN stack. The resulting superstructure exhibits features of considerably smaller dimensions with less pronounced in-plane strain [23].

During the dynamic simulations, the h-BN slider is driven by displacing the top rigid layer with a constant velocity of $v_0 = 5$ m/s in the x direction [Fig. 1(a)] while allowing its vertical rigid vibration. At a temperature of 0 K, the heat generated during shear is dissipated by damping the relative velocities of the atoms in the second h-BN layer (l_2) and the flexible PrisGr layer (l_5) with a damping coefficient $\eta = 1.0$ ps^{-1} in all three directions. This mimics the dissipation through both the slider and the substrate in realistic scenarios with minor effect on the dynamics of atoms at the shear plane (see Ref. [17]). In the finite temperature simulations, Langevin thermostats with the same damping settings are employed. In addition, quasistatic simulations that account for the low velocity sliding regime are also performed. Because of their high computational burden, however, such quasistatic simulations are presented only for certain normal loads. For other simulation details, see Supplementary Materials (SM) [38], Sec. 1.

The interfacial friction is evaluated from the lateral forces acting on the driven layer by the underlying junction during sliding (SM [38], Sec. 2). We find that the heterogeneous polycrystalline interface presents a surprising qualitative mechanistic transition of the frictional dissipation as a function of normal load. At low normal loads ($< \sim 1$ GPa), superlubric behavior is observed (friction coefficients in the range of $-1 \times 10^{-3} - +3 \times 10^{-3}$), where the residual friction originates mainly from the GB seamline [Fig. 2(a)], where a snap-through buckling mechanism of GB protrusions dominates the energy dissipation (Movie 1 [38]). This mechanism was recently rationalized in the context of homogeneous PolyGr interfaces, where shear induced transition between upward and downward (meta-)stable protrusion states of GB dislocations causes energy dissipation. A careful analysis of the various energy dissipation channels in the heterojunction [Fig. 2(c)] reveals that indeed at the low normal load regime, friction is dominated by out-of-plane motion of the GB protrusions. Increasing the normal load suppresses the energy barrier for the snap-through buckling process, resulting in a smooth and nearly dissipationless protrusion

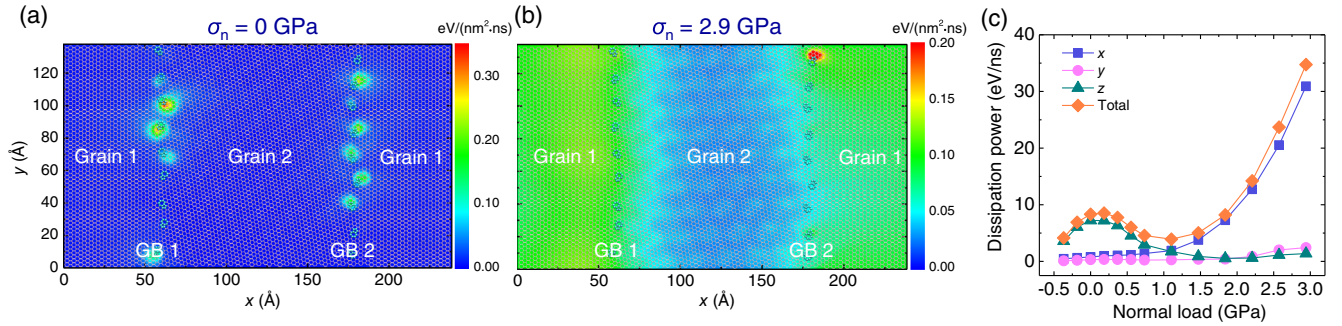

FIG. 2. Energy dissipation analysis. (a) A 2D map of the energy dissipation power density distribution in the damped PrisGr layer l_5 [Fig. 1(a)] at $T = 0$ K under zero normal load. (b) same as (a) at a normal load of 2.9 GPa. (c) Cartesian components and the total energy dissipation power at $T = 0$ K as a function of normal load. See SM [38], Sec. 3 for details regarding the energy dissipation calculation.

inversion, which in the case of homogeneous polycrystalline interfaces results in superlubric motion [red lines in Figs. 3(a) and 3(b)] [20]. Notably, for the heterogeneous polycrystalline interface, a new frictional mechanism emerges at this point, where the energy dissipation is delocalized over the entire surface of grain 1 [Fig. 2(b)], which is aligned with the lattice of the overlying *h*-BN surface and presents large-scale moiré patterns. The energy dissipation channel analysis [Fig. 2(c)] reveals that at this high normal load regime, friction is dominated by in-plane dissipation mostly along the sliding direction. This is further supported by quasistatic (low-velocity limit) and dynamic (high-velocity limit) simulations, both demonstrating a clear stick-slip motion of the entire moiré pattern of grain 1 [Figs. 4(a) and 4(b) and Movies 2 and 3 [38]]. The origin of this superstructure stick-slip behavior is traced back to the fact that with increasing normal-load, the energy difference between the most incommensurate [Fig. 4(a)] and the most

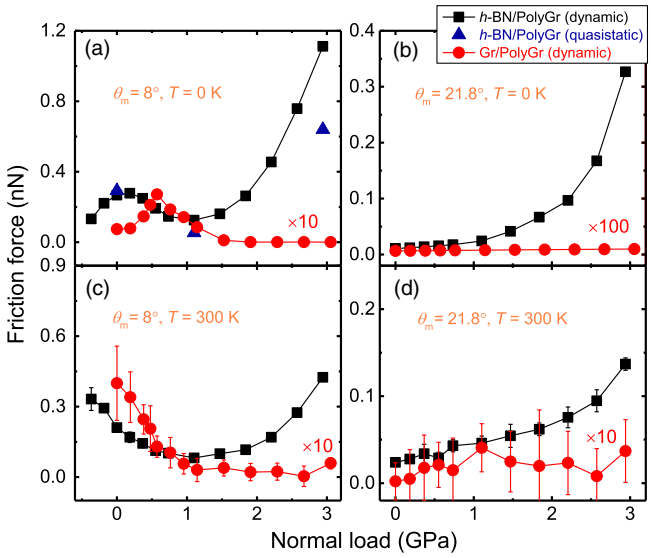

FIG. 3. Friction-load relations. (a) Zero-temperature dependence of the friction force on normal load for the homogeneous PrisGr/PolyGr interface (red) and the heterogeneous *h*-BN/PolyGr interface (black) with an inter-GB misfit angle of $\theta_m = 8°$. (b) same as (a) for a $\theta_m = 21.8°$ interface. (c) same as (a) for a temperature of 300 K. (d) same as (b) for a temperature of 300 K. The red curves are scaled by a factor of 10 in panels (a), (c), and (d), and by a factor of 100 in panel (b) for clarity of the presentation [46]. Results for the $\theta_m = 8°$ homogeneous PolyGr interface [red curves in panels (a) and (c)] below a normal load of 2 GPa are reproduced from Ref. [20].

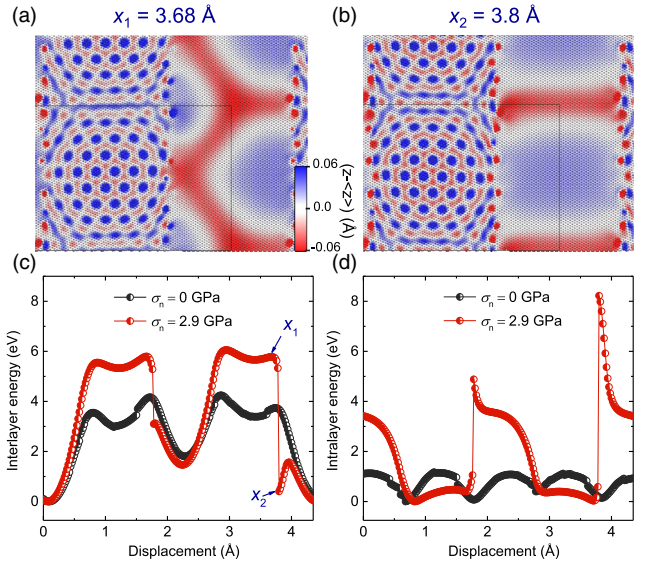

FIG. 4. Quasistatic simulations. (a) and (b) Surface corrugation maps obtain under a normal load of 2.9 GPa at slider displacements of (a) $x_1 = 3.68$ Å and (b) $x_2 = 3.8$ Å, corresponding to the most incommensurate and the most commensurate configurations. The two snapshots depict the moiré superstructure evolution before and after a slip event. In the color bar $\langle z \rangle$ represents the average height of the two grains in the polyGr layer. The corresponding lateral stress distributions are shown in Fig. S16 [38]. (c) and (d) Variation of the interlayer and intralayer energy as a function of slider displacement at zero (black) and under a 2.9 GPa (red) normal loads. The minimal values of the energy profiles are set to zero to emphasize the corrugation of the sliding potential surface.

commensurate [Fig. 4(b)] configurations of grain 1 along the sliding path dramatically increases (red line in Fig. S17 [38]). Notably, the jump between the incommensurate and commensurate configurations [Figs. 4(a) and 4(b)] is associated with a sharp decrease in the interlayer energy [Fig. 4(c), red line] accompanied by a sudden increase in the intralayer counterpart [Fig. 4(d), red line], resulting in the overall increase of the potential energy. This surprisingly large intralayer energy increase results from the annihilation of the moiré triple junction, formed at the intersection of three domain walls [red grooves in Fig. 4(a)], as it reaches the GB. The effect is further enhanced because grain 1 does not accommodate a full moiré period, hence considerable lateral stress develops to achieve commensurability (SM [38], Sec. 4 and Movie 4). In the low-load regime, in turn, the overall interfacial commensurability is lower (SM [38], Sec. 5) resulting in lower in-plane stress [14], which can be relieved via out-of-plane deformations, thus reducing the corresponding commensurate to incommensurate transition barriers [black lines in Figs. 4(c), 4(d), and S17 [38]].

The load induced mechanistic transition discussed above is clearly manifested in the dependence of the dynamical friction force on the normal load. Focusing first on the zero-temperature finite-velocity case, for small intergrain orientation mismatch [$\theta_m = 8°$, Fig. 3(a)], where the GBs are corrugated, the friction force peaks at the low load regime and then reduces up to a load of 1 GPa for both the homogeneous (red) and heterogeneous (black) polycrystalline interfaces. Notably, at the high load regime, these two interfaces exhibit a dramatically different behavior. While in the former further increase of the load results in superlubric behavior, the latter presents a significant increase of the friction due to the moiré superstructure stick-slip mechanism. A qualitatively similar behavior is obtained also in quasistatic simulations accounting for the low-sliding velocity regime [blue triangles in Fig. 3(a)]. The distinction between the two behaviors is even more evident in the case of flat GBs with large intergrain orientation mismatch [$\theta_m = 21.8°$, Fig. 3(b)], where the snap-through buckling mechanism of GB protrusions is absent. In this case, the homogeneous polycrystalline interface exhibits ultralow friction throughout the entire normal load regime considered (red), whereas the heterogeneous junction shows monotonic dependence of the friction on the normal load with a sharp increase above 1 GPa (black) due to moiré stick-slip motion (Movie 5 [38]).

The two frictional mechanisms appear also at room temperature, where thermal fluctuations assist in overcoming the corresponding barriers. In the friction-load diagram [Fig. 3(c)], this translates to a shift of the friction force peak associated with the GB protrusion snap-through buckling mechanism to lower normal loads (red and black), and an overall reduction of the friction enhancement in the high-load regime, where the moiré superstructure stick-slip mechanism dominates for the heterogeneous polycrystalline interface (black). A similar reduction in the high-load friction enhancement regime is also observed for heterogeneous polycrystalline interfaces with flat GBs [Fig. 3(d)].

Interestingly, the load induced transition mechanism from smooth to stick-slip superstructure collective motion revealed herein, resembles the frictional behavior obtained using the Prandtl-Tomlinson model [47–49] for single particle friction, also observed in atomic-scale experiments [50]. This further reflects the generality of the phenomenon that relies on a direct relation between external load and transition barriers inducing an elastic instability that, in turn, introduces friction. This mechanism was absent in previous homogeneous polycrystalline interface simulations [20] due to the relatively high misfit angles between the two grains and the overlying graphitic surface, chosen to prevent locking part of the system in the fully commensurate high-friction state.

We further analyze the moiré superstructure motion in terms of the corresponding in-plane stress variations. Figure 5 presents color maps of the stress evolution along the sliding direction (averaged over the perpendicular

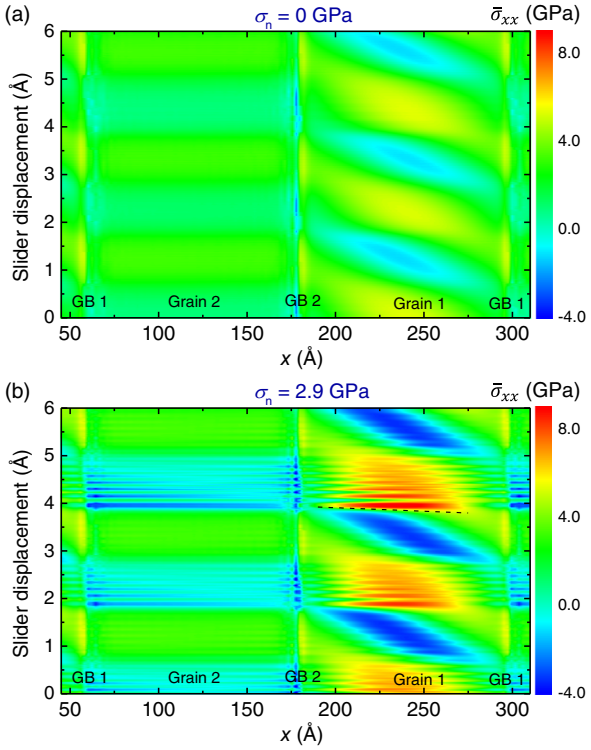

FIG. 5. Two-dimensional stress evolution maps. (a) In-plane stress map along the sliding direction as a function of slider displacement under zero normal load. (b) same as (a) under a normal load of 2.9 GPa. The dashed black line is used to calculate the reflected wave velocity. In both maps, the stress is averaged along the grain direction perpendicular to the sliding path. Positive and negative values indicate expansion and compressive stresses, respectively. The results are obtained for a sliding velocity of $v_0 = 5$ m/s and at a temperature of 0 K.

direction) as a function of the slider displacement at $T = 0$ K. At zero normal load the overall stress is relatively low showing smooth dynamics [Fig. 5(a)]. The slope of the stress fronts occurring over grain 1 correspond to the global velocity of the superstructure (Fig. S15 and Movie 1 [38]). The stress fronts in grain 2 show zero slope indicating a nearly uniform stress distribution along the grain with no apparent propagation. Increasing the load to 2.9 GPa results in an overall increase of the in-plane stress along the sliding direction, where the emergence of the moiré superstructure stick-slip motion over grain 1 becomes clearly evident as abrupt jumps between compression (blue regions) and expansion [red regions in Fig. 5(b)]. Notably, following each slip event, high-frequency features emerge, signifying the occurrence of multiple wave reflections between the two GBs (SM [38], Sec. 7). The corresponding wave velocity can be estimated from the slope of the dashed black line Fig. 5(b) yielding a value of ~3.4 km/s, about a quarter of the Rayleigh velocity of 12.6 km/s predicted for graphene [51]. Grain 2 exhibits a similar behavior but with a lower overall stress and a rather uniform distribution along the grain. The emergent waves lead to an additional energy dissipation channel that accounts for the difference between the finite-velocity and quasistatic friction at the higher normal load considered (Figs. S18 and S19 [38]).

The results presented above facilitate the emergence of a new frictional mechanism based on collective stick-slip motion of moiré superstructures. We demonstrate the phenomenon for polycrystalline interfaces of graphene and *h*-BN, presuming that the interfacial twist angle in at least one of the grains is sufficiently small to yield a moiré superstructure period much larger than the atomic lattice constant. The effect is further enhanced when the small twist angle grain does not accommodate a complete moiré superstructure, resulting in a significant energy difference between the most and least commensurate stacking configurations of the grain. Along with the previously revealed snap-through buckling mechanism of GB protrusions, the frictional behavior of the system exhibits a pronounced nonmonotonic transition between local and collective energy dissipation mechanisms. Since the predicted frictional mechanism relies on geometrically avoided grain boundary crossing of moiré superstructures, it does not depend on the detailed structure and chemistry of the GB seamline and should extend to many other polycrystalline vdW heterojunctions (and twisted homojunctions). Of particular interest would be transition metal dichalcogenide interfaces that possess an even smaller lattice mismatch (~0.2%) [52] than *h*-BN/PolyGr interfaces and are thus expected to present moiré stick-slip dynamics over larger scales. Additionally, possible GB migration processes in these systems are expected to further enrich the superstructure dynamics with interesting manifestation in the interfacial frictional characteristics.

The authors thank J. Fineberg, M. Adda-Bedia, and E. Bouchbinder for helpful discussions. X. G. acknowledges the postdoctoral fellowships of the Sackler Center for Computational Molecular and Materials Science and the Ratner Center for Single Molecule Science at Tel Aviv University. M. U. acknowledges the financial support of the Israel Science Foundation, Grant No. 1141/18 and the ISF-NSFC joint Grant No. 3191/19. O. H. is grateful for the generous financial support of the Israel Science Foundation under Grant No. 1586/17, the Heineman Chair in Physical Chemistry, Tel Aviv University Center for Nanoscience and Nanotechnology, and the Naomi Foundation for generous financial support via the 2017 Kadar Award.

*Corresponding author.
urbakh@tauex.tau.ac.il

[1] A. K. Geim and I. V. Grigorieva, Van der Waals heterostructures, Nature (London) **499**, 419 (2013).
[2] L. Britnell, R. V. Gorbachev, R. Jalil, B. D. Belle, F. Schedin, A. Mishchenko, T. Georgiou, M. I. Katsnelson, L. Eaves, S. V. Morozov *et al.*, Field-effect tunneling transistor based on vertical graphene heterostructures, Science **335**, 947 (2012).
[3] K. Chen, X. Wan, J. Wen, W. Xie, Z. Kang, X. Zeng, H. Chen, and J.-B. Xu, Electronic properties of MoS_2−WS_2 heterostructures synthesized with two-step lateral epitaxial strategy, ACS Nano **9**, 9868 (2015).
[4] K. S. Novoselov, A. Mishchenko, A. Carvalho, and A. H. Castro Neto, 2D materials and van der Waals heterostructures, Science **353**, aac9439 (2016).
[5] F. Xia, H. Wang, D. Xiao, M. Dubey, and A. Ramasubramaniam, Two-dimensional material nanophotonics, Nat. Photonics **8**, 899 (2014).
[6] K. Chaudhary, M. Tamagnone, M. Rezaee, D. K. Bediako, A. Ambrosio, P. Kim, and F. Capasso, Engineering phonon polaritons in van der Waals heterostructures to enhance in-plane optical anisotropy, Sci. Adv. **5**, eaau7171 (2019).
[7] W. Ouyang, O. Hod, and M. Urbakh, Parity-Dependent Moiré Superlattices in Graphene/*h*-BN Heterostructures: A Route to Mechanomutable Metamaterials, Phys. Rev. Lett. **126**, 216101 (2021).
[8] C. Androulidakis, K. Zhang, M. Robertson, and S. Tawfick, Tailoring the mechanical properties of 2D materials and heterostructures, 2D Mater. **5**, 032005 (2018).
[9] J.-W. Jiang and H. S. Park, Mechanical properties of MoS_2/graphene heterostructures, Appl. Phys. Lett. **105**, 033108 (2014).
[10] K. Liu and J. Wu, Mechanical properties of two-dimensional materials and heterostructures, J. Mater. Res. **31**, 832 (2016).
[11] O. Hod, E. Meyer, Q. Zheng, and M. Urbakh, Structural superlubricity and ultralow friction across the length scales, Nature (London) **563**, 485 (2018).
[12] I. Leven, D. Krepel, O. Shemesh, and O. Hod, Robust superlubricity in graphene/*h*-BN heterojunctions, J. Phys. Chem. Lett. **4**, 115 (2013).
[13] Y. Song, D. Mandelli, O. Hod, M. Urbakh, M. Ma, and Q. Zheng, Robust microscale superlubricity in

graphite/hexagonal boron nitride layered heterojunctions, Nat. Mater. **17**, 894 (2018).
[14] D. Mandelli, W. Ouyang, O. Hod, and M. Urbakh, Negative Friction Coefficients in Superlubric Graphite–Hexagonal Boron Nitride Heterojunctions, Phys. Rev. Lett. **122**, 076102 (2019).
[15] M. Liao, P. Nicolini, L. Du, J. Yuan, S. Wang, H. Yu, J. Tang, P. Cheng, K. Watanabe, T. Taniguchi *et al.*, UItra-low friction and edge-pinning effect in large-lattice-mismatch van der Waals heterostructures, Nat. Mater. **21**, 47 (2022).
[16] A. S. de Wijn, A. Fasolino, A. Filippov, and M. Urbakh, Low friction and rotational dynamics of crystalline flakes in solid lubrication, Europhys. Lett. **95**, 66002 (2011).
[17] X. Gao, W. Ouyang, O. Hod, and M. Urbakh, Mechanisms of frictional energy dissipation at graphene grain boundaries, Phys. Rev. B **103**, 045418 (2021).
[18] A. Kavalur and W. K. Kim, Molecular dynamics study on friction of polycrystalline graphene, Comput. Mater. Sci. **137**, 346 (2017).
[19] H. Li and W. K. Kim, Role of multigrain structure on friction of graphene layers, Comput. Mater. Sci. **165**, 23 (2019).
[20] X. Gao, W. Ouyang, M. Urbakh, and O. Hod, Superlubric polycrystalline graphene interfaces, Nat. Commun. **12**, 5694 (2021).
[21] T. A. Sharp, L. Pastewka, and M. O. Robbins, Elasticity limits structural superlubricity in large contacts, Phys. Rev. B **93**, 121402(R) (2016).
[22] D. Dietzel, J. Brndiar, I. Štich, and A. Schirmeisen, Limitations of structural superlubricity: Chemical bonds versus contact size, ACS Nano **11**, 7642 (2017).
[23] D. Mandelli, W. Ouyang, M. Urbakh, and O. Hod, The princess and the nanoscale pea: Long-range penetration of surface distortions into layered materials stacks, ACS Nano **13**, 7603 (2019).
[24] C. R. Woods, L. Britnell, A. Eckmann, R. S. Ma, J. C. Lu, H. M. Guo, X. Lin, G. L. Yu, Y. Cao, R. V. Gorbachev *et al.*, Commensurate–incommensurate transition in graphene on hexagonal boron nitride, Nat. Phys. **10**, 451 (2014).
[25] C. Ophus, A. Shekhawat, H. Rasool, and A. Zettl, Large-scale experimental and theoretical study of graphene grain boundary structures, Phys. Rev. B **92**, 205402 (2015).
[26] A. Shekhawat and R. O. Ritchie, Toughness and strength of nanocrystalline graphene, Nat. Commun. **7**, 10546 (2016).
[27] P. Y. Huang, C. S. Ruiz-Vargas, A. M. van der Zande, W. S. Whitney, M. P. Levendorf, J. W. Kevek, S. Garg, J. S. Alden, C. J. Hustedt, Y. Zhu *et al.*, Grains and grain boundaries in single-layer graphene atomic patchwork quilts, Nature (London) **469**, 389 (2011).
[28] D. W. Brenner, O. A. Shenderova, J. A. Harrison, S. J. Stuart, B. Ni, and S. B. Sinnott, A second-generation reactive empirical bond order (REBO) potential energy expression for hydrocarbons, J. Phys. Condens. Matter **14**, 783 (2002).
[29] J. Tersoff, New empirical approach for the structure and energy of covalent systems, Phys. Rev. B **37**, 6991 (1988).
[30] A. N. Kolmogorov and V. H. Crespi, Registry-dependent interlayer potential for graphitic systems, Phys. Rev. B **71**, 235415 (2005).
[31] I. Leven, I. Azuri, L. Kronik, and O. Hod, Inter-layer potential for hexagonal boron nitride, J. Chem. Phys. **140**, 104106 (2014).
[32] I. Leven, T. Maaravi, I. Azuri, L. Kronik, and O. Hod, Interlayer potential for graphene/*h*-BN heterostructures, J. Chem. Theory Comput. **12**, 2896 (2016).
[33] T. Maaravi, I. Leven, I. Azuri, L. Kronik, and O. Hod, Interlayer potential for homogeneous graphene and hexagonal boron nitride systems: Reparametrization for many-body dispersion effects, J. Phys. Chem. C **121**, 22826 (2017).
[34] W. Ouyang, D. Mandelli, M. Urbakh, and O. Hod, Nanoserpents: Graphene nanoribbon motion on two-dimensional hexagonal materials, Nano Lett. **18**, 6009 (2018).
[35] W. Ouyang, I. Azuri, D. Mandelli, A. Tkatchenko, L. Kronik, M. Urbakh, and O. Hod, Mechanical and tribological properties of layered materials under high pressure: Assessing the importance of many-body dispersion effects, J. Chem. Theory Comput. **16**, 666 (2020).
[36] S. Plimpton, Fast parallel algorithms for short-range molecular dynamics, J. Comput. Phys. **117**, 1 (1995).
[37] W. Ouyang, H. Qin, M. Urbakh, and O. Hod, Controllable thermal conductivity in twisted homogeneous interfaces of graphene and hexagonal boron nitride, Nano Lett. **20**, 7513 (2020).
[38] See Supplemental Material at http://link.aps.org/supplemental/10.1103/PhysRevLett.129.276101 for additional information of simulation methods, friction force calculations, energy dissipation analysis, effects of grain boundary seperation on morié stick-slip phenomenon, interfacial commensurability characterization using the registry index, lateral motion of moiré triple junctions, stress and energy evolution during moiré stick-slip motion, and movies of typical simulations. The Supplemental Material includes Refs. [39–45].
[39] S. Tang, H. Wang, Y. Zhang, A. Li, H. Xie, X. Liu, L. Liu, T. Li, F. Huang, X. Xie *et al.*, Precisely aligned graphene grown on hexagonal boron nitride by catalyst free chemical vapor deposition, Sci. Rep. **3**, 2666 (2013).
[40] O. V. Yazyev and S. G. Louie, Topological defects in graphene: Dislocations and grain boundaries, Phys. Rev. B **81**, 195420 (2010).
[41] Y. Tison, J. Lagoute, V. Repain, C. Chacon, Y. Girard, F. Joucken, R. Sporken, F. Gargiulo, O. V. Yazyev, and S. Rousset, Grain boundaries in graphene on SiC(0001̄) substrate, Nano Lett. **14**, 6382 (2014).
[42] J. Červenka and C. F. J. Flipse, Structural and electronic properties of grain boundaries in graphite: Planes of periodically distributed point defects, Phys. Rev. B **79**, 195429 (2009).
[43] E. Bitzek, P. Koskinen, F. Gähler, M. Moseler, and P. Gumbsch, Structural Relaxation Made Simple, Phys. Rev. Lett. **97**, 170201 (2006).
[44] J. Guénolé, W. G. Nöhring, A. Vaid, F. Houllé, Z. Xie, A. Prakash, and E. Bitzek, Assessment and optimization of the fast inertial relaxation engine (fire) for energy minimization

in atomistic simulations and its implementation in lammps, Comput. Mater. Sci. **175**, 109584 (2020).

[45] I. Leven, R. Guerra, A. Vanossi, E. Tosatti, and O. Hod, Multiwalled nanotube faceting unravelled, Nat. Nanotechnol. **11**, 1082 (2016).

[46] We note that the friction forces are proportional to the sliding potential energy barrier height divided by the corresponding potential profile periodicity. For the homogeneous PolyGr junctions the barriers are lower than those of the corresponding heterojunctions and the sliding periods are larger (∼3.0 nm vs 0.43 nm, respectively), resulting in overall lower friction forces.

[47] L. Prandtl, Ein Gedankenmodell zur kinetischen Theorie der festen Körper, Z. Angew. Math. Mech. **8**, 85 (1928).

[48] G. A. Tomlinson, CVI. A molecular theory of friction, Philos. Mag. **7**, 905 (1929).

[49] A. Vanossi, N. Manini, M. Urbakh, S. Zapperi, and E. Tosatti, Colloquium: Modeling friction: From nanoscale to mesoscale, Rev. Mod. Phys. **85**, 529 (2013).

[50] A. Socoliuc, R. Bennewitz, E. Gnecco, and E. Meyer, Transition from Stick-Slip to Continuous Sliding in Atomic Friction: Entering a New Regime of Ultralow Friction, Phys. Rev. Lett. **92**, 134301 (2004).

[51] B. Zhang, G. Yang, and H. Xu, Instability of supersonic crack in graphene, Physica (Amsterdam) **434B**, 145 (2014).

[52] J. He, K. Hummer, and C. Franchini, Stacking effects on the electronic and optical properties of bilayer transition metal dichalcogenides MoS_2, $MoSe_2$, WS_2, and WSe_2, Phys. Rev. B **89**, 075409 (2014).